Mon. Not. R. Astron. Soc. **000**, 000–000 (0000) Printed 13 January 2010 (MN LATEX style file v2.2)

New insight into the relation between star formation activity and dust content in galaxies

Elisabete da Cunha[1,2,3⋆], Celine Eminian[4], Stéphane Charlot[2,3], Jérémy Blaizot[5]
[1]*Department of Physics, University of Crete, 71003 Heraklion, Greece;*
IESL/Foundation for Research and Technology-Hellas, 71110 Heraklion, Greece.
[2]*UPMC Univ Paris 06, UMR7095, Institut d'Astrophysique de Paris, F-75014, Paris, France.*
[3]*CNRS, UMR7095, Institut d'Astrophysique de Paris, F-75014, Paris, France.*
[4]*Astronomy Centre, University of Sussex, Brighton BN1 9QH, UK.*
[5]*Université de Lyon, Lyon, F-69003, France;*
Université Lyon 1, Observatoire de Lyon, 9 avenue Charles André, Saint-Genis Laval, F-69230, France;
CNRS, UMR 5574, Centre de Recherche Astrophysique de Lyon; Ecole Normale Supérieure de Lyon, Lyon, F-69007, France.

Accepted 2009 December 23. Received 2009 December 13; in original form 2009 August 4

ABSTRACT

We assemble a sample of 3258 low-redshift galaxies from the Sloan Digital Sky Survey Data Release 6 (SDSS DR6) with complementary photometric observations by *GALEX*, 2MASS and *IRAS* at far-ultraviolet and infrared wavelengths. We use a recent, simple but physically motivated model to interpret the observed spectral energy distributions of the galaxies in this sample in terms of statistical constraints on physical parameters describing the star formation history and dust content. The focus on a subsample of 1658 galaxies with highest signal-to-noise ratio (S/N) observations enables us to investigate most clearly several strong correlations between various derived physical properties of galaxies. In particular, we find that the typical dust mass $M_{\rm d}$ of a galaxy forming stars at a rate ψ can be estimated remarkably well using the formula $M_{\rm d} = (1.28 \pm 0.02) \times 10^7 \, (\psi/M_\odot \, {\rm yr}^{-1})^{1.11 \pm 0.01} \, M_\odot$ over at least three orders of magnitude in both quantities. We also find that the dust-to-stellar mass ratio, the ratio of dust mass to star formation rate and the fraction of dust luminosity contributed by the diffuse interstellar medium (ISM) all correlate strongly with specific star formation rate. A comparison with recent models of chemical and dust evolution of galaxies suggests that these correlations could arise, at least in part, from an evolutionary sequence. As galaxies form stars, their ISM becomes enriched in dust, while the drop in gas supply makes the specific star formation rate decrease. Interestingly, as a result, a young, actively star-forming galaxy with low dust-to-gas ratio may still be highly dusty (in the sense of a high dust-to-stellar mass ratio) because it contains large amounts of interstellar gas. This may be important for the interpretation of the infrared emission from young, gas-rich star-forming galaxies at high redshift. The results presented in this paper should be especially useful to improve the treatment of the ISM properties of galaxies in semi-analytic models of galaxy formation. Our study also provides a useful local reference for future statistical studies of the star formation and dust properties of galaxies at high redshifts.

Key words: dust, extinction – galaxies: ISM – galaxies: stellar content – galaxies: statistics – galaxies: evolution.

1 INTRODUCTION

Interstellar dust and star formation activity are strongly linked in galaxies. Dust grains condense in the cold envelopes of evolved stars and in supernova ejecta. In return, they favour the formation of molecular hydrogen, shield the newly-formed molecules from ultraviolet radiation and participate in the formation and cooling of molecular clouds, which collapse to form new stars.

Studies of the ultraviolet, optical and near-infrared emission from large samples of local galaxies have shed some light on the relation between star formation activity and dust content. Such studies show that, in general, galaxies with the highest star formation rates also suffer the highest ultraviolet and optical attenuation (e.g., Kauffmann et al. 2003b; Brinchmann et al. 2004). However, observations at ultraviolet, optical and near-infrared wavelengths set only

⋆ E-mail: dacunha@physics.uoc.gr

limited constraints on the dust content of galaxies. New insight into the dust properties requires observations at mid- and far-infrared wavelengths, where the dust re-radiates the energy absorbed from starlight. The first studies of this kind combined ultraviolet and optical observations of large samples of nearby galaxies with empirical estimates of the total infrared luminosity computed from observations with the *Infrared Astronomical Satellite* (*IRAS*) at 12, 25, 60 and 100 μm (e.g. Wang & Heckman 1996; Hopkins et al. 2001; Sullivan et al. 2001; Kong et al. 2004). Other recent studies have taken this (largely empirical) approach a step further by developing consistent models of galactic spectral energy distributions at ultraviolet, optical and infrared wavelengths (e.g. Silva et al. 1998; Dopita et al. 2005). These sophisticated models combine the spectral evolution of stellar populations with detailed calculations of the transfer of starlight through the interstellar medium in galaxies. Such models, however, are not optimised to interpret the observations of large samples of galaxies.

Recently, da Cunha et al. (2008) proposed a simple, physically motivated model to interpret consistently the ultraviolet, optical and infrared observations of large samples of galaxies in terms of statistical constraints on physical parameters pertaining to the stars, gas and dust. By design, this model is less sophisticated than other existing radiative transfer models. In return, it allows one to interpret efficiently the spectral energy distributions of large samples of galaxies in terms of statistical constraints on a minimal set of adjustable physical parameters. da Cunha et al. (2008) used this model to derive median-likelihood estimates of the stellar mass, star formation rate, dust attenuation and dust mass from the observed ultraviolet, optical and infrared spectral energy distributions of 66 galaxies in the *Spitzer* Infrared Nearby Galaxy Sample (SINGS, Kennicutt et al. 2003). For these galaxies, the dust-to-stellar mass ratio appears to correlate strongly with specific star formation rate (i.e. the star formation rate divided by the total stellar mass), confirming the expectation that dust mass and star formation rate are tightly related in galaxies.

In the present paper, we investigate further the relation between star formation activity and dust content by studying the properties of a much larger sample of 3258 star-forming galaxies, for which photometric observations are available at ultraviolet, optical and infrared wavelengths. We use the model of da Cunha et al. (2008) to derive median-likelihood estimates of several physical parameters of each galaxy in this sample, such as the total stellar mass, dust mass star formation rate and fractional contribution of different dust components to the total infrared luminosity. We then focus on a sub-sample of 1658 galaxies with highest signal-to-noise ratio (S/N) photometry from the far-ultraviolet to the far-infrared. The large size of this sample allows us to study in unprecedented detail the relations between specific star formation rate, dust mass and dust-to-gas ratio already identified in the SINGS sample by da Cunha et al. (2008). We find that, in particular, the typical dust mass $M_{\rm d}$ of a galaxy forming stars at a rate ψ can be remarkably well estimated using the formula $M_{\rm d} = (1.28 \pm 0.02) \times 10^7 \, (\psi / M_{\odot} \, {\rm yr}^{-1})^{1.11 \pm 0.01} \, M_{\odot}$.

We interpret our results in the framework of recent models of chemical and dust evolution of galaxies by Calura et al. (2008). These models provide a means of predicting the time evolution of the stellar and dust content of galaxies with different star formation histories. We conclude from this that the relations between specific star formation rate and dust content exhibited by the galaxies in our sample could be regarded, at least in part, as an evolutionary sequence.

The paper is organised as follows. We first describe the matched *GALEX*-SDSS-2MASS-*IRAS* sample in Section 2. In Section 3, we outline the method used to derived statistical estimates of the total stellar mass, dust mass, star formation rate and fractional contribution of different dust components to the total infrared luminosity for each galaxy in this sample. We present the relations between these various derived quantities in Section 4. In Section 5, we discuss some potential biases of our approach. We also compare our results with the predictions of different models to illustrate the implications of our study for the evolution of the dust content of star-forming galaxies. Section 6 summarises our conclusions.

2 THE GALAXY SAMPLE

In this work we analyse a galaxy sample obtained by cross-correlating the Sloan Digital Sky Survey Data Release 6 (SDSS DR6) main spectroscopic sample with photometric catalogues at ultraviolet (from the *Galaxy Evolution Explorer*, *GALEX*), near-infrared (from the Two Micron All Sky Survey, 2MASS) and far-infrared (from the *Infrared Astronomical Satellite*, *IRAS*) wavelengths.

2.1 Optical photometry

The SDSS DR6 spectroscopic sample (Adelman-McCarthy et al. 2008) contains 792,680 galaxies with known redshifts to a Petrosian r-band magnitude limit $r < 17.77$. Optical photometry in the $ugriz$ bands (at 3557, 4825, 6261, 7672 and 9097 Å, respectively) is available for these galaxies. We use the SDSS 'model magnitudes' in these bands, which reflect the integrated light from the whole galaxy and are the best suited to comparisons with total photometry from *GALEX*, 2MASS and *IRAS* at ultraviolet and infrared wavelengths. We stress that such consistent multi-wavelength photometry is a key requirement in the interpretation of the spectral energy distributions of the galaxies in Section 3.

Many fundamental parameters of the galaxies of the SDSS DR6 spectroscopic sample have been derived from the spectroscopic data (e.g. Brinchmann et al. 2004), and are publicly available in an online database[1]. We use this information to restrict our sample to galaxies classified as 'star-forming' according to their emission lines. Active Galactic Nuclei (AGNs) in the sample are eliminated when at least one of two criteria are met: (i) the presence of broad emission lines from high-velocity gas around the AGN (e.g. Brinchmann et al. 2004); (ii) the presence of narrow emission lines with intensity ratios characteristic of an AGN in the Baldwin, Phillips & Terlevich diagram (BPT; Baldwin et al. 1981), according to the criterion of Kauffmann et al. (2003a)[2]. If the emission lines are highly attenuated, the BPT diagnostic may fail to identify an obscured AGN (in Section 5.3, we discuss the possible contamination of our sample by optically thick AGN). Observations in the X-rays or in the mid-infrared can be used to detect AGN in this case.

[1] http://pc-66.astro.up.pt/∼jarle/GASS/

[2] The BPT diagram allows one to distinguish star-forming galaxies from AGN on the basis of the degree of ionisation of the gas by comparing the narrow-line ratios [O III]λ 5007 Å/Hβ against [N II]λ 6584 Å/Hα.

2.2 Ultraviolet photometry

To supplement SDSS DR6 spectroscopic data with ultraviolet measurements, we cross-correlate the sample with the latest data release from *GALEX* (Martin et al. 2005; Morrissey et al. 2005). *GALEX* is an all-sky survey providing images of the galaxies in two photometric bands: the far-ultraviolet (*FUV*, at 1520 Å) and the near-ultraviolet (*NUV*, at 2310 Å). To match the SDSS and *GALEX* catalogues, we use a search radius of 4 arcsec around the SDSS position (data kindly provided in advance of publication by David Schiminovich). We require a detection in at least one of the two *FUV* and *NUV* bands. We retain galaxies which have a single *GALEX* detection within the search radius, i.e., we eliminate objects for which two or more *GALEX* detections may exist for the same SDSS source. We adopt *GALEX* FUV and NUV 'automags', which use a Kron aperture defined by the profile of each galaxy in each band, and are designed to recover the total flux.

At ultraviolet wavelengths, Galactic foreground extinction is particularly important. Therefore, we apply Galactic reddening corrections to the *GALEX* magnitudes (Seibert et al. 2005): $A_{\rm FUV} = 8.29\ E(B-V)$ and $A_{\rm NUV} = 8.18\ E(B-V)$, where the colour excess $E(B-V)$ is determined from the dust reddening maps of Schlegel et al. (1998). Although observations at longer wavelengths are less affected by Galactic extinction, we also correct the observed optical magnitudes of Section 2.1 and near-infrared magnitudes of Section 2.3 using the same method.

2.3 Near-infrared photometry

We further supplement our sample with near-infrared photometry in the JHK_s bands (at 1.25, 1.65 and 2.17 μm, respectively) from the 2MASS (Skrutskie et al. 2006) All Sky Extended Source Catalog (XSC). We cross-identify the SDSS DR6 spectroscopic sample and the 2MASS XSC within a search radius of 5 arcsecs around the SDSS coordinates. Only sources with no artefacts and which are not in close proximity to a large nearby galaxy are retained. Concerning the photometry, we follow the recommendations in the User's Guide to the 2MASS All-Sky Data Release[3] to include most of the integrated flux from the galaxies while providing accurate colours: we adopt K20 fiducial isophotal elliptical aperture magnitudes for galaxies with $K_s < 13$, and fixed 7 arcsec circular aperture magnitudes for fainter galaxies.

2.4 Mid- and far-infrared photometry

We now turn to the most original feature of our sample: the inclusion of mid- and far-infrared photometry obtained with *IRAS* (Beichman et al. 1988). Observations with *IRAS* are rather limited in sensitivity, but they have the advantage of providing an all-sky survey at 12, 25, 60 and 100 μm.[4] We cross-correlate our sample with both the *IRAS* Point Source Catalogue (PSCz; Saunders et al. 2000) and the *IRAS* Faint Source Catalogue v2.0 (FSC; Moshir 1989). The PSCz catalogue is a complete and uniform galaxy catalogue assembled from the *IRAS* Point Source Catalogue (Beichman et al. 1988) and supplemented by various redshift surveys. It contains 15,411 galaxies with measured redshifts to a depth of 0.6 Jy at 60 μm. The Faint Source Catalogue contains 173,044 sources to a depth of roughly 0.25 Jy at 60 μm. Low Galactic latitude regions ($|b| < 20^\circ$) are excluded from this catalogue because of the contamination by foreground Galactic sources at this detection limit. For both catalogues, we rely on the quoted data quality flags to select sources having a good flux quality at 60 μm and at least a moderate flux quality at 100 μm; detections at 12 and 25 μm are not strictly required. To increase the reliability of the sample, we exclude observations which are confusion-limited or contaminated by cirrus emission.

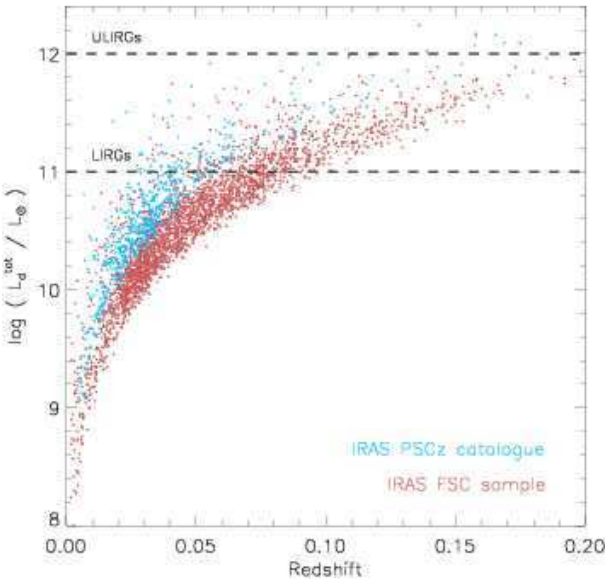

Figure 1. Total infrared luminosity $L_{\rm d}^{\rm tot}$ from equation (1) plotted against redshift for galaxies in the matched *GALEX*-SDSS-2MASS-*IRAS* described in Section 2. Galaxies belonging to the *IRAS* PSCz catalogue (blue symbols) are distinguished from those belonging to the *IRAS* FSC catalogue (red symbols).

We cross-correlate the SDSS sample with the *IRAS* PSCz and *IRAS* FSC catalogues using the same criteria as Pasquali et al. (2005), i.e., we discard *IRAS* sources with more than one SDSS-matched object within a search radius of 30 arcsec. For the PSCz catalogue (with redshift information), this criterion appears to cause only about 1 per cent of the infrared sources to be assigned the wrong SDSS counterpart. The contamination may be higher in the case of the lower-quality FSC catalogue. Using simulated data, Pasquali et al. (2005) estimate that the percentage of wrong cross-identifications is at most 1.5 per cent for a matching radius of 30 arcsec.

2.5 Final sample

Our final *GALEX*-SDSS-2MASS-*IRAS* sample is composed of 3258 galaxies from the PSCz and FSC catalogues at redshifts $z \leqslant 0.22$ (see Fig. 2a). To summarise, the galaxies in this sample have:

- ultraviolet fluxes in at least one of the *FUV* and *NUV GALEX* bands;
- optical $ugriz$ fluxes from SDSS;
- near-infrared JHK_s fluxes from 2MASS;
- 60- and 100-μm flux densities from *IRAS* (some galaxies also have 12- and 25-μm measurements).

[3] http://www.ipac.caltech.edu/2mass/releases/allsky/doc/

[4] In practice, most measurements at 12 and 25 μm are upper limits on the flux density, and we do not include them in our spectral fits. Only about 3 per cent of the galaxies in the sample are detected in all 4 *IRAS* bands.

We note that, for consistency, all fluxes used in our study are designed to be *total fluxes*, which do not require aperture corrections. For this reason, we also choose not to include SDSS spectroscopic information available for these galaxies, which is restricted to the inner 3-arcsec diameter aperture sampled by the SDSS spectroscopic fibre aperture. At the low redshifts of our galaxies, this limited spatial sampling could severely bias estimates of the star formation rate and dust content (Kewley et al. 2005). In addition, spectroscopic quantities pertaining to a restricted central area cannot be compared directly with multi-wavelength photometric quantities describing the whole galaxy.

It is instructive to examine the typical infrared luminosity $L_{\rm d}^{\rm tot}$ of the galaxies in our sample. For this purpose, we compute $L_{\rm d}^{\rm tot}$ from the 60- and 100-μm *IRAS* flux densities F_ν^{60} and F_ν^{100} using the empirical formula (Helou et al. 1988)

$$L_{\rm d}^{\rm tot} = F_{\rm c}\, L_{\rm FIR}\,, \tag{1}$$

where

$$L_{\rm FIR} = 1.26\times10^{-14}(2.58\,F_\nu^{60}+F_\nu^{100})\,4\pi d_{\rm L}^2\,. \tag{2}$$

Here, $d_{\rm L}$ is the luminosity distance in m, F_ν^{60} and F_ν^{100} are in Jy, and $L_{\rm d}^{\rm tot}$ and $L_{\rm FIR}$ are in W. We compute the correction factor F_c to obtain $L_{\rm d}^{\rm tot}$ from $L_{\rm FIR}$ in equation (1) following the empirical prescription of Helou et al. (1988), which depends on the F_ν^{60}/F_ν^{100} ratio, and assuming a dust emissivity index $\beta = 2$. The resulting median correction for our sample is $F_c = 1.35$.

In Fig. 1, we plot the total dust infrared luminosity $L_{\rm d}^{\rm tot}$ computed in this way as a function of redshift. A large fraction of the galaxies in our sample (about 22 per cent) have $L_{\rm d}^{\rm tot} > 10^{11}\ L_\odot$. Such galaxies are usually referred to as 'luminous infrared galaxies' (LIRGs). About 1 per cent of the galaxies of our sample have $L_{\rm d}^{\rm tot} > 10^{12}\ L_\odot$. These galaxies with extremely high infrared luminosities are usually referred to as 'ultra-luminous infrared galaxies' (ULIRGs). This type of galaxies has been the object of extensive studies (e.g. Soifer et al. 1987; Veilleux et al. 1995, 1999; Rigopoulou et al. 1999; Cao et al. 2006; Armus et al. 2007). In the local universe, most ULIRGs are observed to be the results of interactions and mergers. Visual inspection of the SDSS optical images confirms that ULIRGS in our sample also have disturbed morphologies.

In Fig. 2, we compare the properties of our sample with the overall properties of the SDSS star-forming galaxy sample. Fig. 2a shows that galaxies in our sample tend to lie at lower redshifts than the bulk of SDSS star-forming galaxies. This results from the required detection by low-sensitivity *IRAS* observations. Fig. 2b further shows that galaxies in our sample tend to have typically redder $g-r$ colours than SDSS star-forming galaxies. This is most probably a consequence of the higher dust content of our galaxies, which makes them detectable by *IRAS*. In fact, Obrić et al. (2006, see their figure 19) point out that SDSS galaxies detected by *IRAS* have systematically higher dust attenuation than the average SDSS star-forming galaxy. The difference in the distributions of r-band absolute magnitude M_r in Fig. 2c is more subtle to interpret. This is illustrated by Fig. 2d, where we plot M_r in different redshift bins for both samples. At redshifts $z < 0.12$, galaxies in our sample are typically brighter than SDSS star-forming galaxies. This is because SDSS galaxies with intrinsically faint r-band magnitudes are too faint in the infrared to be detected by *IRAS*. At redshifts $z > 0.12$, the SDSS and *IRAS* detection limits both correspond to similarly bright galaxies.

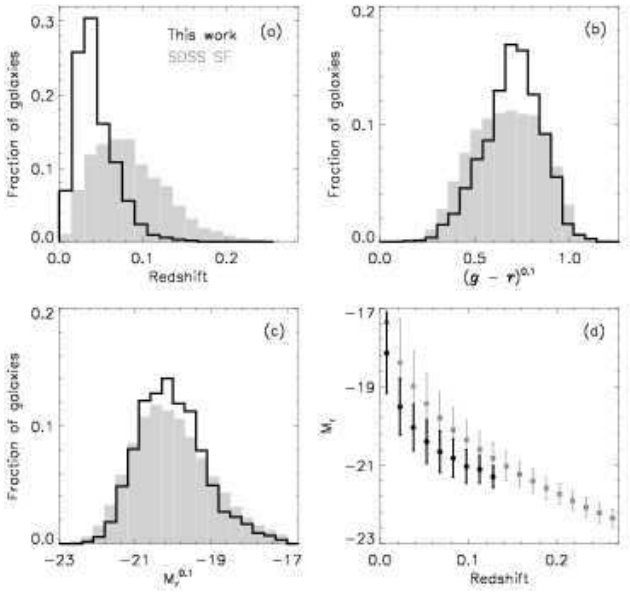

Figure 2. Properties of the SDSS DR6 star-forming galaxies (in grey) and the matched *GALEX*-SDSS-2MASS-*IRAS* subsample considered in this work (in black). The histograms show the normalised distributions of the following parameters: (a) Redshift, z; (b) Galaxy $g-r$ colour, k-corrected to redshift $z = 0.1$; (c) Absolute r-band model magnitude, k-corrected to redshift $z = 0.1$, $\mathrm{M}_r^{0.1}$. Panel (d) shows the mean r-band absolute magnitude, M_r, in different redshift bins for both samples (the error bars represent the standard deviation $\pm\sigma$ in each bin).

3 STATISTICAL CONSTRAINTS ON PHYSICAL PARAMETERS

In this Section, we use the simple model of da Cunha et al. (2008) to extract star formation histories and dust contents from the ultraviolet, optical and infrared observations of the galaxy sample described in Section 2. We first briefly summarise the model. Then, we describe the statistical approach used to derive median-likelihood estimates of physical parameters from the available data.

3.1 Description of the model

The simple, physically motivated model of da Cunha et al. (2008) allows us to interpret the mid- and far-infrared spectral energy distributions of galaxies consistently with the emission at ultraviolet, optical and near-infrared wavelengths. We briefly recall the main features of this model.

We compute the emission by stars in galaxies using the latest version of the Bruzual & Charlot (2003) population synthesis code (Charlot & Bruzual, in preparation). This code predicts the spectral evolution of stellar populations in galaxies from far-ultraviolet to far-infrared wavelengths and at ages between 1×10^5 and 2×10^{10} yr, for different metallicities, initial mass functions (IMFs) and star formation histories. In this work, we adopt the Chabrier (2003) Galactic-disc IMF.

The emission from stars is attenuated using the simple two-component dust model of Charlot & Fall (2000). This accounts for the fact that stars are born in dense molecular clouds with typical lifetimes of 10^7 yr; at later ages, stars migrate to the ambient (diffuse) ISM. Thus, the light produced by stars younger than 10^7 yr is attenuated by dust in the birth clouds and in the ambient ISM,

while the light produced by older stars is attenuated only by dust in the ambient ISM. The model of Charlot & Fall (2000) uses an 'effective absorption' curve for each component, $\hat{\tau}_\lambda \propto \lambda^{-n}$. The slope n reflects both the optical properties and the spatial distribution of the dust. Following Charlot & Fall (2000), we adopt for the ambient ISM

$$\hat{\tau}_\lambda^{\rm ISM} = \mu \hat{\tau}_V (\lambda/5500 \text{ Å})^{-0.7} , \quad (3)$$

where $\hat{\tau}_V$ is the total effective V-band absorption optical depth of the dust seen by young stars inside birth clouds, and $\mu = \hat{\tau}_V^{\rm ISM}/(\hat{\tau}_V^{\rm BC} + \hat{\tau}_V^{\rm ISM})$ is the fraction of this contributed by dust in the ambient ISM. For the stellar birth clouds, we adopt:

$$\hat{\tau}_\lambda^{\rm BC} = (1-\mu) \hat{\tau}_V (\lambda/5500 \text{ Å})^{-1.3} . \quad (4)$$

We use this prescription to compute the total energy absorbed by dust in the birth clouds and in the ambient ISM; this energy is re-radiated by dust at infrared wavelengths. By analogy with da Cunha et al. (2008), we define the total dust luminosity re-radiated by dust in the birth clouds and in the ambient ISM as $L_{\rm d}^{\rm BC}$ and $L_{\rm d}^{\rm ISM}$, respectively. The total luminosity emitted by dust in the galaxy is then

$$L_{\rm d}^{\rm tot} = L_{\rm d}^{\rm BC} + L_{\rm d}^{\rm ISM} . \quad (5)$$

We distribute $L_{\rm d}^{\rm BC}$ and $L_{\rm d}^{\rm ISM}$ in wavelength over the range from 3 to 1000 μm using 4 main components (see da Cunha et al. 2008 for detail):

- the emission from polycyclic aromatic hydrocarbons (PAHs; i.e. mid-infrared emission features),
- the mid-infrared continuum emission from hot dust with temperatures in the range 130–250 K,
- the emission from warm dust in thermal equilibrium with adjustable temperature in the range 30–60 K,
- the emission from cold dust in thermal equilibrium with adjustable temperature in the range 15–25 K.

In stellar birth clouds, the relative contributions to $L_{\rm d}^{\rm BC}$ by PAHs, the hot mid-infrared continuum and warm dust are kept as adjustable parameters. These clouds are assumed not to contain any cold dust. In the ambient ISM, the contribution to $L_{\rm d}^{\rm ISM}$ by cold dust is kept as an adjustable parameter. The relative proportions of the other 3 components are fixed to the values reproducing the mid-infrared cirrus emission of the Milky Way. da Cunha et al. (2008) find that the above minimum number of components is required to account for the infrared spectral energy distributions of galaxies in a wide range of star formation histories.

3.2 Median-likelihood estimates of physical parameters

The model summarised in Section 3.1 allows us to derive statistical estimates of galaxy physical parameters, such as the stellar mass, star formation rate and dust mass, from simultaneous fits of ultraviolet, optical and infrared observations. To achieve this, we adopt a Bayesian approach similar to that used by da Cunha et al. (2008) to interpret the spectral energy distributions of SINGS galaxies.

3.2.1 Model library

We build large libraries of stochastic models at different redshifts $z = 0.00$, 0.05, 0.10, 0.15 and 0.20.

At each redshift, we generate a random library of stellar population models for wide ranges of star formation histories, metallicities and dust contents. Each star formation history is parameterised in terms of an underlying continuous model with exponentially declining star formation rate, on top of which are superimposed random bursts (see also Kauffmann et al. 2003b). The models are distributed uniformly in metallicity between 0.2 and 2 times solar. The attenuation by dust is randomly sampled by drawing the total effective V-band absorption optical depth, $\hat{\tau}_V$, between 0 and 6, and the fraction of this contributed by dust in the ambient ISM, μ, between 0 and 1 (see da Cunha et al. 2008 for more details on the prior distributions of these parameters). For each model, we compute the fraction of the total energy absorbed by dust in the diffuse ISM, f_μ. We also compute the specific star formation rate averaged over the last $t_8 = 10^8$ yr,

$$\psi_{\rm S}(t) = \frac{\int_{t-t_8}^{t} dt' \psi(t')}{t_8 M_*(t)} , \quad (6)$$

where $M_*(t)$ is the stellar mass at time t.

In parallel, at each redshift, we generate a random library of infrared spectra for wide ranges of dust temperatures and fractional contributions by different dust components to the total infrared luminosity. The fraction of total dust luminosity contributed by the diffuse ISM, $f_\mu = L_{\rm d}^{\rm ISM}/L_{\rm d}^{\rm tot}$, and the fractional contribution by warm dust in thermal equilibrium to the total dust luminosity of the birth clouds, $\xi_{\rm W}^{\rm BC}$, are uniformly distributed between 0 and 1; the fractions of luminosity contributed by the other components in the birth clouds, $\xi_{\rm MIR}^{\rm BC}$ (hot mid-infrared continuum) and $\xi_{\rm PAH}^{\rm BC}$ (PAHs), are randomly drawn from prior distributions such that $\xi_{\rm W}^{\rm BC} + \xi_{\rm MIR}^{\rm BC} + \xi_{\rm PAH}^{\rm BC} = 1$. We distribute uniformly the temperature of warm dust in thermal equilibrium in the birth clouds, $T_{\rm W}^{\rm BC}$, between 30 and 60 K, and the temperature of cold dust in thermal equilibrium in the diffuse ISM, $T_{\rm C}^{\rm ISM}$, between 15 and 25 K. Finally, we distribute uniformly the contribution by cold dust to the total infrared luminosity of the ISM, $\xi_{\rm C}^{\rm ISM}$, between 0.5 and 1.

We compute the dust mass associated to each model in the library of infrared spectra as

$$M_{\rm d} = 1.1 \, (M_{\rm W}^{\rm BC} + M_{\rm W}^{\rm ISM} + M_{\rm C}^{\rm ISM}) , \quad (7)$$

where $M_{\rm W}^{\rm BC}$, $M_{\rm W}^{\rm ISM}$ and $M_{\rm C}^{\rm ISM}$ are the masses of the dust components in thermal equilibrium (warm dust in the birth clouds and the ambient ISM and cold dust in the ambient ISM). The multiplying factor 1.1 accounts for the small contribution by stochastically heated dust (see da Cunha et al. 2008 for detail). The mass $M_{\rm d}(T_{\rm d})$ of dust in thermal equilibrium at the temperature $T_{\rm d}$ is estimated from the corresponding far-infrared luminosity, $L_\lambda^{T_{\rm d}}$, using the relation (Hildebrand 1983)

$$L_\lambda^{T_{\rm d}} = 4\pi \, M_{\rm d}(T_{\rm d}) \, \kappa_\lambda \, B_\lambda(T_{\rm d}) , \quad (8)$$

where κ_λ is the dust mass absorption coefficient and $B_\lambda(T_{\rm d})$ the Planck function of temperature $T_{\rm d}$. Following da Cunha et al. (2008), we adopt $\kappa_\lambda \propto \lambda^{-\beta}$, with $\beta = 1.5$ for warm dust and $\beta = 2.0$ for cold dust, normalised to $\kappa_{850} = 0.77$ g^{-1} cm^2 at 850 μm (Dunne et al. 2000).

We combine the stochastic libraries of attenuated stellar spectra and dust emission spectra at each redshift by associating models corresponding to similar values of f_μ (to within some uncertainty interval $\delta f_\mu = 0.15$) in the two libraries, which we scale to the same total dust luminosity $L_{\rm d}^{\rm tot}$. For each combined spectrum, we compute the synthetic photometry in the *GALEX* FUV and NUV, SDSS $ugriz$, 2MASS JHK_s and *IRAS* 12-, 25-, 60- and 100-μm bands.

3.2.2 Corrections applied to the observed fluxes

In the redshift range of the sample described in Section 2, prominent optical nebular emission lines can significantly affect the observed galaxy fluxes in the SDSS gri bands. The model spectra we use to interpret these data do not include nebular emission lines. Therefore, to interpret the optical fluxes of observed galaxies with these models, we first need to correct the observed SDSS gri magnitudes for potential contamination by nebular emission lines (e.g., Kauffmann et al. 2003b). We use the corrections inferred by Jarle Brinchmann (private communication) from fits of the stellar continuum emission of each SDSS optical spectrum with Bruzual & Charlot (2003) models (we assume for simplicity that the correction derived in this way within the aperture sampled by the SDSS fibre applies to the galaxy as a whole).

We also compute *k*-corrections to the ultraviolet, optical and near-infrared magnitudes of each galaxy in the sample. To minimise these, we *k*-correct the magnitudes from the galaxy redshift to the closest redshift of the model grid described in Section 3.2.1, i.e., $z = 0.00$, 0.05, 0.10, 0.15 or 0.20 (we use the version v3 of the KCORRECT code of Blanton et al. 2003). This procedure cannot be extended to the *IRAS* 12-, 25-, 60- and 100-μm flux densities, to which we do not apply any *k*-correction. We do not expect this to have any noticeable influence on our results, given the large effective width of the *IRAS* filter response functions and the relatively large observational uncertainties in these bands.

To account for the uncertainties linked to the *k*-correction and emission-line correction, we add the following errors to the quoted flux uncertainties: 2 per cent for *GALEX*, 2MASS, and SDSS z bands, and 1.5 per cent for the SDSS gri bands. For the less accurate SDSS u-band photometry, we take an overall observational uncertainty of 10 per cent.

3.2.3 Spectral fits

We perform spectral fits by comparing the observed spectral energy distribution of a galaxy to every model in the library at the corresponding redshift. Specifically, for each observed galaxy, we compute the χ^2 goodness of fit of each model. A model is characterised by a set of randomly drawn physical parameters. We build the likelihood distribution of any given physical parameter for the observed galaxy by weighting the value of that parameter in each model by the probability $\exp(-\chi^2/2)$. We take our final estimate of the parameter to be the median of the likelihood distribution, and the associated confidence interval to be the 16th–84th percentile range.

We use this approach to derive the likelihood distributions of several physical parameters of the galaxies in our sample, based on fits of the *GALEX FUV* and *NUV*, SDSS $ugriz$, 2MASS JHK_s and *IRAS* 12-, 25-, 60- and 100-μm fluxes. We focus particularly on: the star formation rate averaged over the last 10^8 yr, ψ; the stellar mass, M_*; the specific star formation rate, $\psi_{\rm S} = \psi/M_*$; the dust mass, $M_{\rm d}$; the total luminosity of the dust, $L_{\rm d}^{\rm tot}$, and the fraction of this contributed by the diffuse ISM, f_μ.

We first check how well the model can reproduce the observed spectral energy distributions of the galaxies in our sample. The histograms in Fig. 3 show, for each photometric band, the distribution of the difference between the observed luminosity $L_\nu^{\rm obs}$ and the best-fit model luminosity $L_\nu^{\rm mod}$, in units of observational error σ. Overall, the model provides remarkably consistent fits to the observed ultraviolet, optical and infrared luminosities of the galaxies. Fig. 3 shows small systematic offsets in the g, r and z bands,

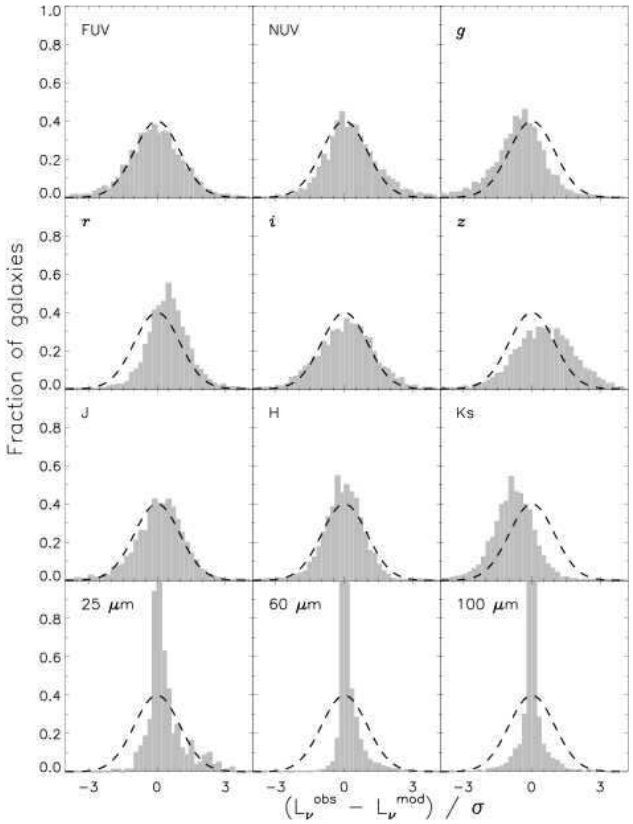

Figure 3. Distribution of the difference between observed luminosity $L_\nu^{\rm obs}$ and best-fit model luminosity $L_\nu^{\rm mod}$, in units of the observational error σ, for the galaxies in the matched *GALEX*-SDSS-2MASS-*IRAS* sample described in Section 2. Each panel refers to a different photometric band, as indicated. For reference, the black dashed curve shows a Gaussian distribution with unit standard deviation. The best-fit model for each galaxy was selected by fitting as many fluxes as available in the following bands: *GALEX* (*FUV* and *NUV*), SDSS ($ugriz$), 2MASS (JHK_s), and *IRAS* (12, 25, 60 and 100 μm).

corresponding to an overestimate of the g-band flux and underestimates of the r- and z-band fluxes of the order of 0.01 mag. These offsets may originate from a deficiency in stellar population synthesis models, further worsened by the potential contamination of the g and r bands by minor emission lines, which we neglected in our corrections of Section 3.2.2. We note that the magnitude of these offsets is of the order of the uncertainties in the SDSS AB calibration[5]. In the near-infrared, there is a tendency for the model to slightly overestimate the observed K_s-band luminosity (by an amount corresponding to about 0.10 mag). This offset is well within the uncertainties of current stellar population synthesis models for this spectral region. We have checked that these offsets have a negligible influence on our results.

To illustrate the quality of these fits, we show in Fig. 4 three examples of the best-fit spectral energy distributions of galaxies spanning wide ranges in star formation and dust properties in our sample, from quiescent, moderately dusty (IRAS F15105+5959, top panel) to actively star-forming, highly dusty (IRAS F09253+1724, bottom panel). The middle panel shows the spectral energy distribution of a galaxy corresponding roughly to

[5] see http://www.sdss.org/DR7/algorithms/fluxcal.html#sdss2ab

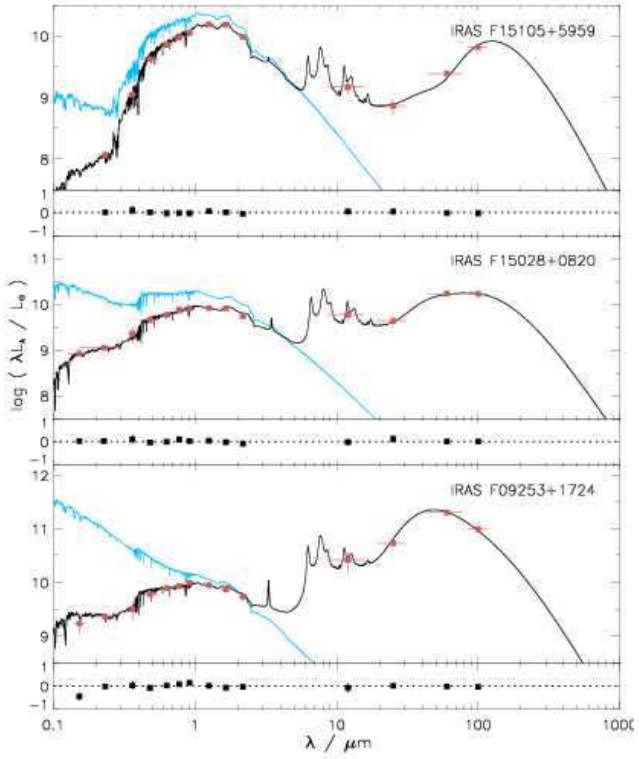

Figure 4. Best-fit models (in black) to the observed spectral energy distributions (in red) of 3 galaxies spanning wide ranges in star formation and dust properties in the matched *GALEX*-SDSS-2MASS-*IRAS* sample described in Section 2: from quiescent, moderately dusty (top panel) to actively star-forming, highly dusty (bottom panel). In each panel, the blue line shows the unattenuated stellar spectrum. The red squares show the observed broad-band luminosities (*GALEX FUV*, *NUV*; SDSS $ugriz$; 2MASS JHK_s; *IRAS* 12, 25, 60 and 100 μm) with their errors as vertical bars and the widths of the filters as horizontal bars. The fit residuals $(L_\lambda^{\rm obs} - L_\lambda^{\rm mod})/L_\lambda^{\rm obs}$ are shown at the bottom of each panel.

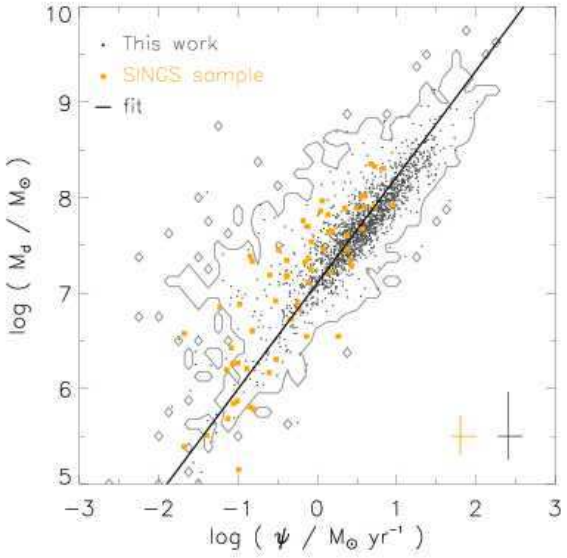

Figure 5. Median-likelihood estimate of the dust mass, $M_{\rm d}$, versus that of the star formation rate averaged over the last 10^8 yr, ψ, for the matched *GALEX*-SDSS-2MASS-*IRAS* sample described in Section 2 (in grey) and the SINGS galaxies (in orange). The grey contour shows the distribution of the full matched sample of 3258 galaxies, while grey points show the distribution of the sub-sample of 1658 galaxies with highest-S/N photometry in all bands (see text). The median error bars for each sample are indicated in the lower-right corner. These correspond to the median 16th–84th percentile range of the likelihood distributions in $M_{\rm d}$ and ψ. The black line shows a linear fit to the grey points, computed as the bisector of the least-square regression lines on each axis.

the median star formation and dust properties of the sample (IRAS F15028+0820).

4 THE RELATION BETWEEN STAR FORMATION ACTIVITY AND DUST CONTENT IN GALAXIES

The method described in Section 3 above allows us to derive statistical constraints on the star formation rate averaged over the last 10^8 yr, ψ, the stellar mass, M_*, the total dust luminosity, $L_{\rm d}^{\rm tot}$, the fraction of this contributed by dust in the diffuse interstellar medium, f_μ, and the total dust mass, $M_{\rm d}$, for the 3258 galaxies in the matched *GALEX*-SDSS-2MASS-*IRAS* sample described in Section 2.

In Fig. 5, we show the resulting relation between dust mass $M_{\rm d}$ and star formation rate ψ. The grey contour shows the distribution for the full sample, while grey points show the distribution of a sub-sample of 1658 galaxies with highest-S/N photometry at ultraviolet, optical and infrared wavelengths. This high-S/N sub-sample includes only galaxies with relative photometric errors less than 2σ larger than the sample mean in each band. Also shown in the lower-right corner of Fig. 5 are the median errors in ψ and $M_{\rm d}$, derived from the likelihood distributions of these parameters for all the galaxies in the sample.

The correlation between dust mass and star formation rate is remarkably tight in Fig. 5, spanning 4 orders of magnitude in both ψ and $M_{\rm d}$. We perform a linear fit to the grey points (i.e., the highest-S/N subsample) by computing the bisector of two least-square regression lines (Isobe et al. 1990): one in $M_{\rm d}$ as a function of ψ, and one in ψ as a function of $M_{\rm d}$. This gives (black line in Fig. 5)

$$M_{\rm d} = (1.28 \pm 0.02) \times 10^7 \, (\psi / M_\odot \ {\rm yr}^{-1})^{1.11 \pm 0.01} \, M_\odot \, . \qquad (9)$$

The uncertainties quoted in this expression are formal ones derived by taking into account the confidence range in each ψ and $M_{\rm d}$ measurement. These uncertainties are much smaller than the intrinsic scatter of the relation (about 0.5 dex in $M_{\rm d}$). Equation (9) can thus be used to estimate the 'typical' dust mass in a galaxy, based on the star formation rate. To our knowledge it is the first time that such an expression is calibrated for a large sample of galaxies.

We have investigated the extent to which the SDSS, *GALEX* and *IRAS* selections of our sample may introduce a bias in the relation between star formation rate and dust mass derived from Fig. 5. We used for this the library of stochastic models described in Section 3.2.1. Since these models are normalised to total stellar mass (da Cunha et al. 2008), we assigned a random stellar mass (and scaled dust mass and star formation rate) to each model in the library. We drew the stellar masses uniformly in $\log(M_*/M_\odot)$ between 8.5 and 11.5, to be consistent with the distribution of galaxy stellar masses in our sample. For each model in the library, we computed the expected *GALEX*, SDSS and *IRAS* magnitudes in different redshift bins from $z = 0$ to $z = 0.20$. Then, we applied the

same selection criteria as used for our observed sample to the model library. These selection criteria introduce minimum detectable stellar mass, dust mass and star formation rate. We find that, for example, at the low-redshift end of our sample ($z = 0.0025$), the *IRAS* flux limit tends to exclude galaxies with $\log(M_{\rm d}/M_{\odot}) < 4.5$. At the typical redshift of our sample, $z = 0.05$, the combination of SDSS and *IRAS* selections sets a minimum detectable dust mass of about 10^7 $M_{\odot}$ and a minimum star formation rate of about 0.01 $M_{\odot}$ yr^{-1} (it also introduces serious incompleteness for galaxies with star formation rates less than 1 $M_{\odot}$ yr^{-1}). We have checked that these selection effects do not affect significantly the empirical relation between the star formation rate and dust mass derived from Fig. 5, which is dominated by more massive galaxies (including only galaxies with $\psi > 1\,M_{\odot}$ yr^{-1} and $M_{\rm d} > 10^7 M_{\odot}$ leaves the derived slope unchanged in equation 9).

In Fig. 5, we also plot for comparison the dust masses and star formation rates derived by da Cunha et al. (2008) for the SINGS galaxies (orange symbols). These nearby galaxies follow the same relation as the galaxies in the matched *GALEX*-SDSS-2MASS-*IRAS* sample studied here and extend to slightly lower dust masses and star formation rates[6]. We note that, at fixed star formation rate, the SINGS galaxies tend to have slightly larger dust masses than the galaxies in our sample. This is likely to result from the different selection criteria of the SINGS sample. The typical error bars in $M_{\rm d}$ and ψ are smaller for the SINGS galaxies than for the sample studied here, because a wider collection of observational constraints (especially in the mid-infrared) were available to da Cunha et al. (2008).

In an attempt to understand which observations set the main constraints on dust mass, we have investigated how the median-likelihood estimates of $M_{\rm d}$ correlate with a wide range of galaxy colours. We find that $M_{\rm d}$ correlates most strongly with the $F_{\nu}^{100}/F_{\nu}^{g}$ colour, where F_{ν}^{100} is the flux density in the *IRAS* 100-μm band and F_{ν}^{g} that in the SDSS g band. The Spearman rank coefficient for this correlation is $r_S = 0.56$, indicating a positive correlation at the 23σ level for this sample size (we note that the correlation is not improved by the inclusion of an ultraviolet band such as *GALEX* FUV). The reason for this correlation is that $F_{\nu}^{100}/F_{\nu}^{g}$ traces the primary contributor to $M_{\rm d}$: cold dust in the diffuse ISM ($M_{\rm C}^{\rm ISM}$ in eq. 7). This component is also mainly responsible for the attenuation of the emission from stars older than 10^7 yr, which dominate the SDSS g-band light, and it is the main contributor to the emission at 100 μm (a more detailed discussion of the set of observables necessary to constrain $M_{\rm d}$ can be found in Section 3.2.2 of da Cunha et al. 2008).

In Fig. 6, we explore the relations between specific star formation rate $\psi_{\rm S}$ and three particularly interesting physical properties of the galaxies in our sample: the dust-to-stellar mass ratio $M_{\rm d}/M_*$, the ratio of dust mass to star formation rate $M_{\rm d}/\psi$, and the fraction f_{μ} of the total infrared luminosity $L_{\rm d}^{\rm tot}$ contributed by dust in the diffuse ISM. As in Fig. 5, grey contours show the relations for the full sample of 3258 galaxies, while individual points show the relations for the 1658 galaxies with highest-S/N photometry. The top panels of Fig. 6 indicate that $M_{\rm d}/M_*$, $M_{\rm d}/\psi$ and f_{μ} are all strongly correlated with $\psi_{\rm S}$: the Spearman rank coefficients for the full sample are $r_S = 0.84$, -0.60 and -0.66, respectively, indicating that the correlations are significant at more than 20σ level for this sample size (similar results are obtained when using only the high-S/N subsample). It is important to check that stellar mass is not the main driver for these strong correlations. To verify this, in the bottom panels of Fig. 6, we show differences in the same quantities as in the top panels for pairs of galaxies closely matched in stellar mass (we have included all possible galaxy pairs for any stellar mass M_* in the full sample). Specifically, for each galaxy pair, we plot the difference in specific star formation rate between the two galaxies, $[\Delta \log(\psi_{\rm S}/{\rm yr}^{-1})]$, against the difference in dust-mass to stellar-mass ratio, $[\Delta \log(M_{\rm d}/M_*)]$, the difference in ratio of dust mass to star formation rate, $[\Delta \log(M_{\rm d}/\psi)]$, and the difference in fraction of total infrared luminosity contributed by the diffuse ISM $[\Delta f_{\mu}]$. The fact that the strong correlations subsist from the top to the bottom panels of Fig. 6 demonstrates that stellar mass is not the main driver of these correlations.

It is of interest to check the extent to which the properties of galaxies in Fig. 6 actually depend on stellar mass. Several studies have shown that the star formation activity of a galaxy tends to decrease with increasing stellar mass (e.g., Brinchmann et al. 2004). In Fig. 7, we plot $M_{\rm d}/M_*$, $M_{\rm d}/\psi$ and f_{μ} as a function of $\psi_{\rm S}$ for 3 different stellar-mass ranges chosen to contain roughly similar numbers of galaxies. The distributions in the various quantities on the y-axis and their median values are displayed in the right-hand panels. Fig. 7 shows that the relation between $M_{\rm d}/M_*$ and $\psi_{\rm S}$ depends little on stellar mass, with only a slight tendency for the less massive galaxies to have somewhat higher $M_{\rm d}/M_*$. Also, the quantity $M_{\rm d}/\psi$, which traces the dust-to-gas ratio, tends to increase slightly with stellar mass. The quantity displaying the strongest dependence on stellar mass in Fig. 7 is the fraction f_{μ} of the total infrared luminosity contributed by dust in the diffuse ISM: the median value of this parameter increases from 0.5 for low-mass galaxies to 0.7 for high-mass ones. We note that the 3 stellar-mass bins considered here span only a small dynamic range in M_*, which may not be enough to reveal the full dependence of the considered properties on stellar mass. It is tempting to interpret the relations of Figs. 6 and 7 as evolutionary sequences, where the build-up of stellar mass would be accompanied by gas consumption and dust enrichment. We return to this point Section 5.4 below.

We have also checked that the non-detection in the 12- and 25-μm *IRAS* bands of most galaxies in the sample (Section 2.4) has a negligible influence on the results of Fig. 6. This is illustrated by the blue triangles in the top panels of the figure, which mark galaxies with complete *IRAS* information in the 12-, 25-, 60- and 100-μm bands. As expected, the median errors in the derived parameters of these galaxies are typically smaller than those for the full sample (as indicated in the upper-right corner of each diagram). Fig. 6 shows that galaxies with complete *IRAS* information follow the same trends as the rest of the sample. Thus, the availability of only the 60- and 100-μm *IRAS* flux densities for most galaxies in the sample does not appear to systematically bias the results.

The strength of the correlations between $\psi_{\rm S}$ and $M_{\rm d}/M_*$, $M_{\rm d}/\psi$ and f_{μ} in Fig. 6 suggests that the specific star formation rate is a fundamental diagnostic of the ISM properties in galaxies. The left-hand panels of Fig. 6 show that, for example, the galaxies with highest specific star formation rate are also the most dust-rich. The reason for this can be best understood with the help of the middle panels. In these diagrams, $M_{\rm d}/\psi$ may be regarded as a proxy for the dust-to-gas ratio, since ψ is tightly related to the gas mass (H I + H_2) by virtue of the Schmidt-Kennicutt law (Schmidt 1959; Kennicutt 1998a). The inverse correlation between $M_{\rm d}/\psi$ and $\psi_{\rm S}$ suggests that the dust-to-gas ratio is larger in galaxies with low spe-

[6] da Cunha et al. (2008) have checked that the dust masses of the SINGS galaxies derived using the model described in Section 3 above are typically within 50 per cent of those estimated by Draine et al. (2007) using a more sophisticated physical dust model.

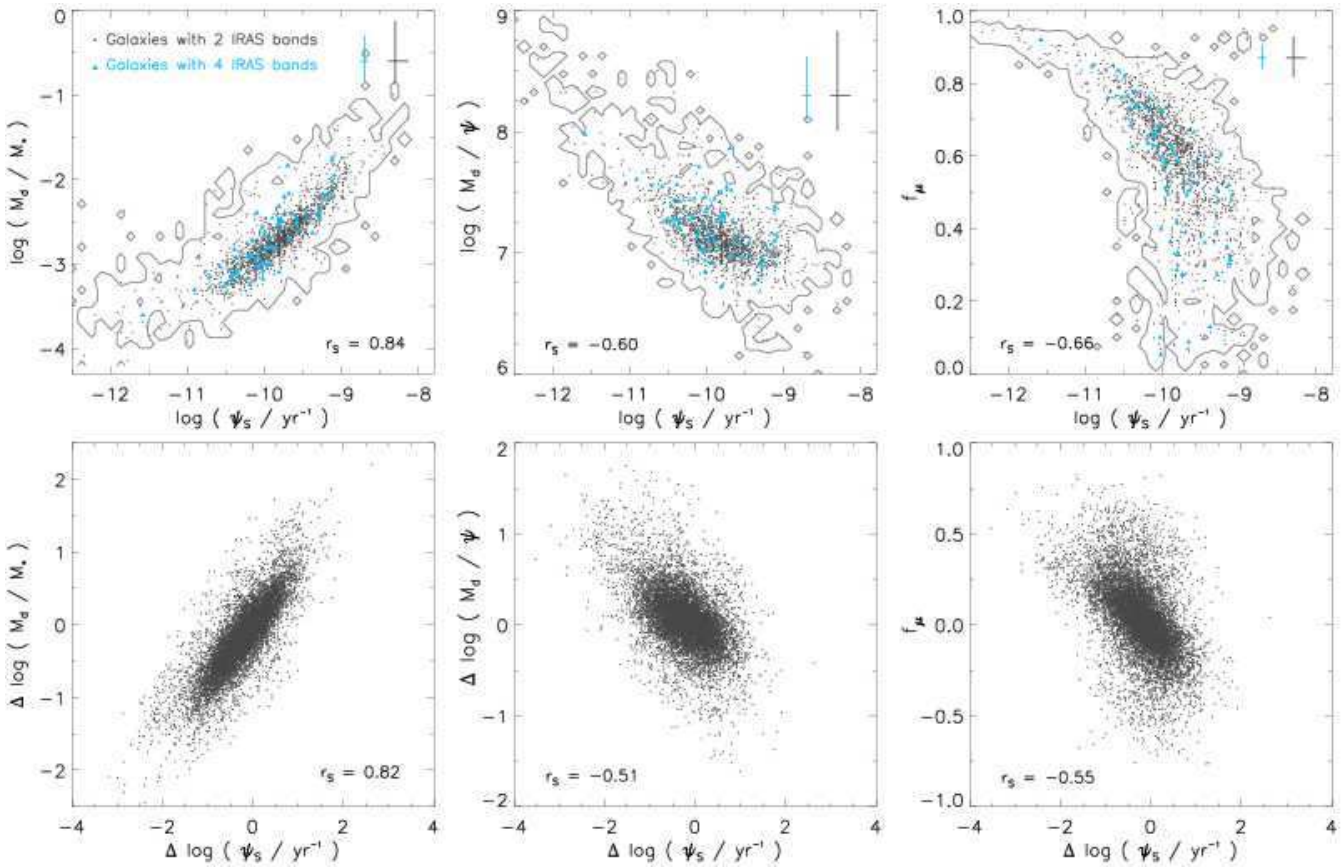

Figure 6. *Top:* Median-likelihood estimates of 3 galaxy properties against specific star formation rate, $\psi_{\rm S}$. *Left panel*: ratio of dust mass to stellar mass, $M_{\rm d}/M_*$. *Middle panel*: ratio of dust mass to star formation rate, $M_{\rm d}/\psi$ (which may be used as a proxy for the dust-to-gas ratio; see Section 4). *Right panel*: fraction of total infrared luminosity contributed by dust in the ambient ISM, f_μ. In each panel, the grey contour shows the distribution of the full matched *GALEX*-SDSS-2MASS-*IRAS* sample described in Section 2, while the points show the distribution of the sub-sample of 1658 galaxies with highest-S/N photometry in all bands. The blue triangles show galaxies with complete *IRAS* information in the 12-, 25-, 60- and 100-μm bands. The error bars represent the median confidence ranges in each parameter. *Bottom:* differences in the same quantities as in the top panels for pairs of galaxies closely matched in stellar mass (see text for detail). The Spearman rank coefficient r_S is indicated in each panel.

cific star formation rate, which have presumably exhausted their gas reservoir. In contrast, galaxies with high specific star formation rate and hence large gas reservoirs tend to have lower dust-to-gas ratio [we note that supernovae and young asymptotic-giant-branch (AGB) stars will produce large amounts of new dust in these galaxies; see e.g. Dwek 1998]. The left-hand panels of Fig. 6 show that, as a result, a young, actively star-forming galaxy with low dust-to-gas ratio may still be highly dusty (in the sense of a high $M_{\rm d}/M_*$) because it contains large amounts of interstellar gas (see also Section 5.4 below). Finally, the right-hand panels of Fig. 6 show that stellar birth clouds are the main contributors to dust heating in actively star-forming galaxies, while in more quiescent galaxies, the bulk of dust emission arises from the heating of dust by older stars in the diffuse interstellar medium. This trend was previously noted for SINGS galaxies by da Cunha et al. (2008).

We may attempt to combine the above estimates of the dust mass $M_{\rm d}$ for the galaxies in our sample with gas-mass estimates derived from the star formation rate ψ via the Schmidt-Kennicutt law, to constrain the dust-to-gas ratio. The Schmidt-Kennicutt takes the form (Kennicutt 1998b)

$$\Sigma_{\rm SFR} = (2.5 \pm 0.7) \times 10^{-4}\, \Sigma_{\rm H}^{1.4\pm0.15}\,, \qquad (10)$$

where $\Sigma_{\rm SFR}$ is the surface density of star formation, expressed in $M_\odot\,{\rm yr}^{-1}\,{\rm kpc}^{-2}$, and $\Sigma_{\rm H}$ is the surface mass density of H I+H_2 gas, expressed in $M_\odot\,{\rm pc}^{-2}$. This formula was derived using a Salpeter (1955) IMF with lower and upper cut-offs 0.1 and 100 $M_\odot$. We adjust the scaling coefficient by a factor of 1.6 down to account for the fact that the da Cunha et al. (2008) model used here relies on a Chabrier (2003) IMF with same cut-offs. We compute $\Sigma_{\rm SFR}$ for the galaxies in the high-S/N subsample studied above by dividing our estimates of ψ by the area defined by the minor and major axes of the r-band isophote at 25 mag arcsec^{-2} (see Section 5.2). We then compute $\Sigma_{\rm H}$ and hence $M_{\rm H}$ using equation (10).

In Fig. 8, we plot the dust-to-gas ratio $M_{\rm d}/M_{\rm H}$ derived in this way against the stellar mass M_* and the dust attenuation optical depth in the diffuse ISM $\mu\hat{\tau}_V$ for the galaxies in the high-S/N subsample. The median errors in $M_{\rm d}/M_{\rm H}$ are quite large. Yet, this ratio appears to correlate with both M_* ($r_S = 0.33$; 13σ significance level) and $\mu\hat{\tau}_V$ ($r_S = 0.50$; 20σ significance level). The correlation with M_* is consistent with the tight correlation between stellar mass and gas-phase metallicity for SDSS star-forming galaxies (e.g. Tremonti et al. 2004). In fact, the strong correlation between dust-to-gas ratio and gas-phase metallicity has been noted in several previous studies (e.g. Issa et al. 1990; Schmidt & Boller 1993; Lisenfeld & Ferrara 1998). We note that the relation between

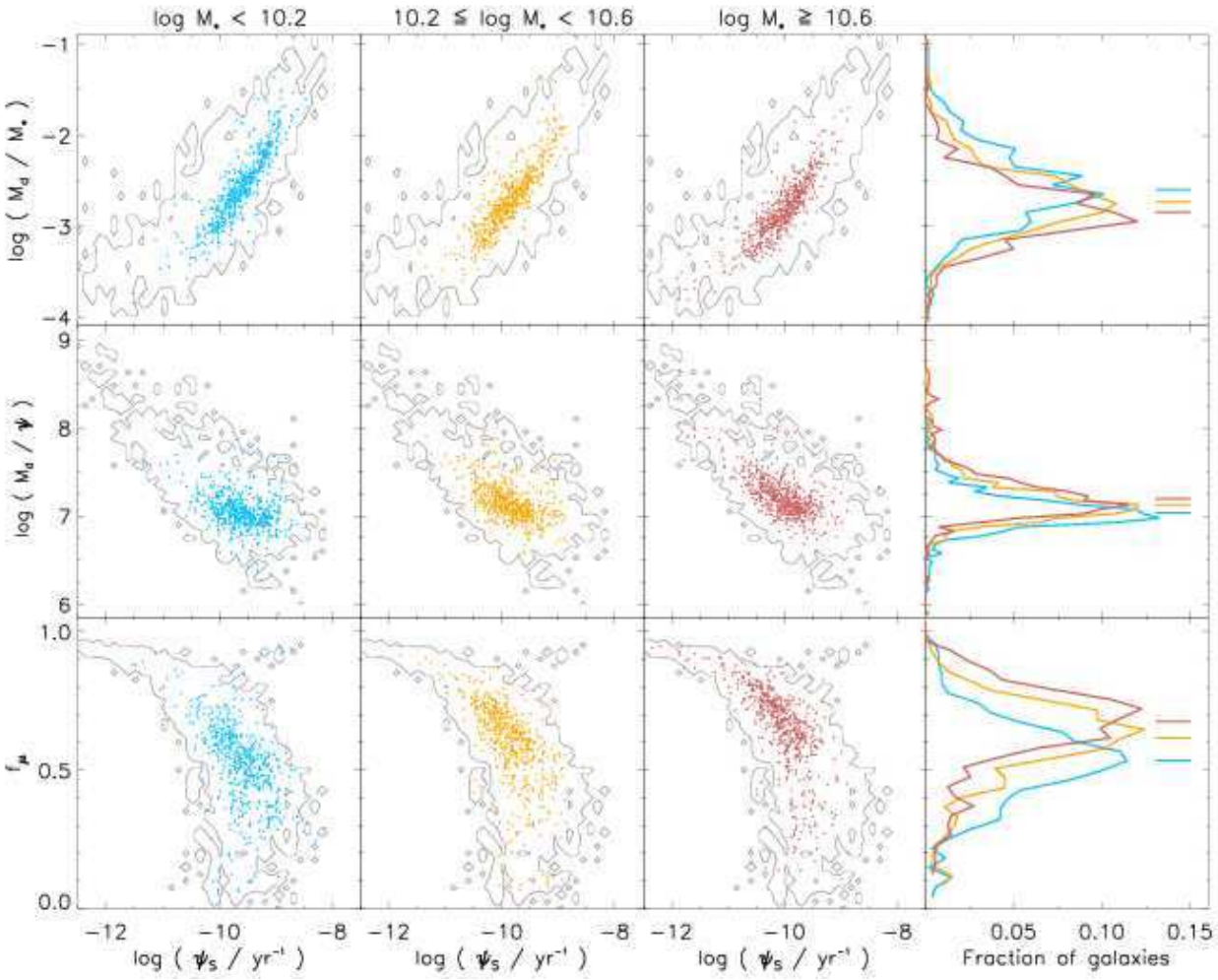

Figure 7. Same relations as in the top panels of Fig. 6 plotted in 3 stellar-mass ranges: $\log(M_*/M_\odot) < 10.2$ (blue); $10.2 \leqslant \log(M_*/M_\odot) < 10.6$ (orange); $\log(M_*/M_\odot) \geqslant 10.6$ (red). The right-hand panels show the corresponding distributions of the dust-to-stellar mass ratio $M_{\rm d}/M_*$, the ratio of dust mass to star formation rate $M_{\rm d}/\psi$ and the fraction f_μ of total infrared luminosity contributed by dust in the ambient ISM, along with their median values. The contours are the same as in the top panels of Fig. 6.

$M_{\rm d}/M_{\rm H}$ and $\mu\hat{\tau}_V$ in Fig. 8 has too much scatter for the dust optical depth in the diffuse ISM to be used as a reliable proxy for the dust-to-gas ratio in galaxies.

5 DISCUSSION

In this section, we briefly mention model uncertainties and discuss potential biases introduced by inclination effects and the presence of obscured AGNs in the results derived in the previous sections. We also compare these results with the predictions of models of chemical and dust evolution to illustrate the implications of our study for the evolution of star-forming galaxies.

5.1 Model uncertainties

The da Cunha et al. (2008) model used in Section 3 to derive the physical properties of galaxies in the matched *GALEX*-SDSS-2MASS-*IRAS* sample relies on a combination of the latest version of the Bruzual & Charlot (2003) population synthesis code and the simple two-component dust model of Charlot & Fall (2000). Recently, Conroy et al. (2009) have investigated the uncertainties inherent to such models, in particular, those arising from poorly understood phases of stellar evolution (blue horizontal branch stars, blue straggler stars, thermally pulsing AGB stars), the IMF and the properties of dust in the interstellar medium.[7] Uncertainties linked to the IMF will affect our analysis in the same way as pointed out by these authors. In our case, the uncertainties linked to stellar evolution are somewhat minimized by the fact that blue-straggler and

[7] We note that Conroy et al. (2009) inappropriately refer to the Charlot & Fall (2000) model as a 'uniform screen of dust'. In reality, by design, the effective attenuation curve in the Charlot & Fall (2000) model reflects the probability density for the absorption of photons emitted in all directions by stars in all locations within a galaxy (see their eq. [18]). The shape of this curve – which is the quantity primarily constrained by observations – is controlled by the combination of the optical properties and the spatial distribution of the dust. Allowing for variations in this shape therefore allows one to explore variations in the spatial distribution of the dust in a galaxy (as exemplified in section 4 of Charlot & Fall 2000).

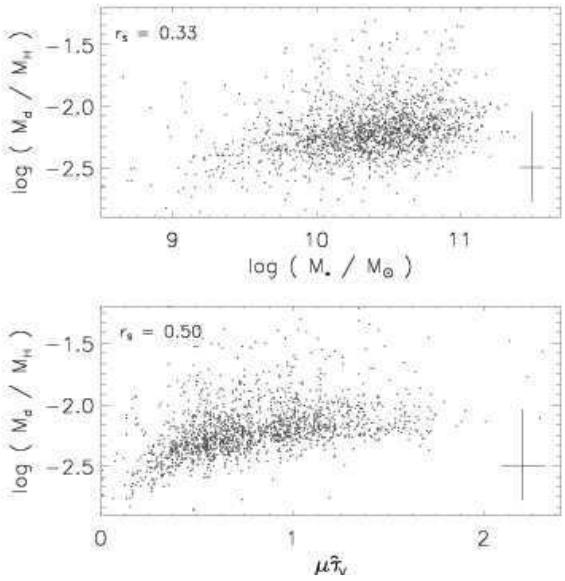

Figure 8. *Top*: ratio of dust mass $M_{\rm d}$ to gas mass, $M_{\rm H} = M_{\rm H\,I} + M_{\rm H_2}$, plotted against the stellar mass M_* for the 1658 galaxies with highest-S/N photometry in the matched *GALEX*-SDSS-2MASS-*IRAS* sample described in Section 2. *Bottom*: $M_{\rm d}/M_{\rm H}$ ratio plotted against the dust attenuation optical depth in the diffuse ISM, $\mu\hat{\tau}_V$, for the same sample. The median error bars are indicated in the lower-right corner of each panel.

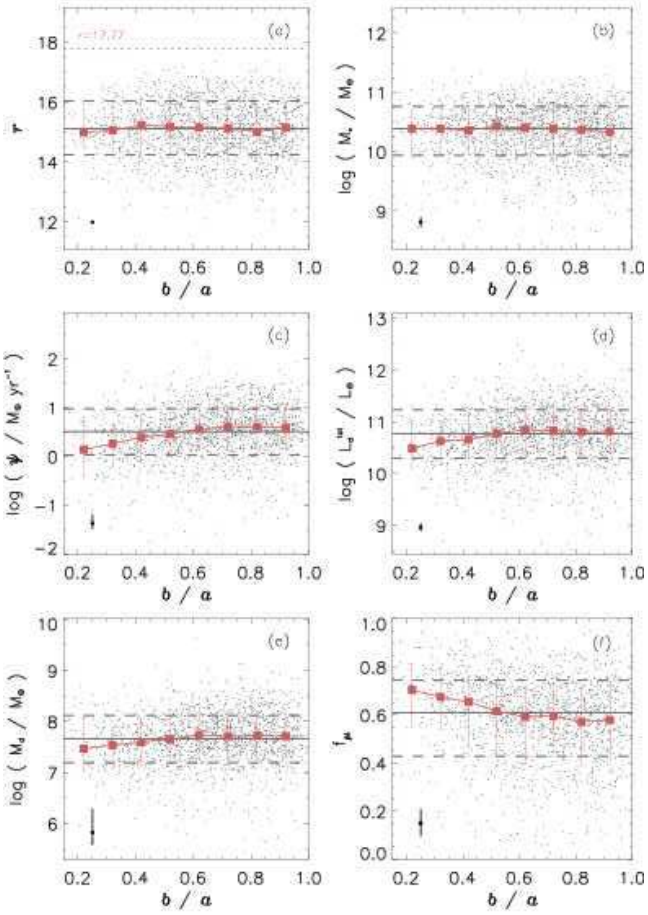

Figure 9. Galaxy properties plotted against ratio of minor to major axes b/a (used as a proxy for inclination) for the 1658 galaxies with highest-S/N photometry in the matched *GALEX*-SDSS-2MASS-*IRAS* sample described in Section 2: (a) apparent r-band magnitude, r; (b) stellar mass, M_*; (c) star formation rate averaged over the last 10^8 yr, ψ; (d) total infrared luminosity, $L_{\rm d}^{\rm tot}$; (e) dust mass, $M_{\rm d}$; (f) fraction of $L_{\rm d}^{\rm tot}$ contributed by dust in the diffuse ISM, f_μ. Red squares and error bars indicate the median values and 16th–84th percentile ranges in bins of b/a. For reference, the horizontal solid and dashed grey lines indicate the median value and 16th–84th percentile range for the whole sample (i.e. including all inclinations). The median observational error in r is indicated in the lower-left corner of panel (a). In each panel from (b) to (f), the median confidence interval in the likelihood estimates of the considered parameter is indicated in the lower-left corner.

horizontal-branch stars have a negligible contribution to the emission from star-forming galaxies. Also the version of the Bruzual & Charlot (2003) models used here rely on the improved, empirically calibrated models of Marigo & Girardi (2007) to better account for the contribution by thermally pulsing AGB stars to the near-infrared emission from galaxies (see Bruzual 2007). We refer the reader to the original studies of Charlot & Fall (2000) and da Cunha et al. (2008) for discussions of the uncertainties in the dust model (e.g., spatial distribution and optical properties of dust grains; typical lifetime of giant molecular clouds) and their influence on the ultraviolet and infrared emission from galaxies.

5.2 The effect of inclination

The model used in Section 3 to derive the physical properties of galaxies in the matched *GALEX*-SDSS-2MASS-*IRAS* sample is limited to angle-averaged spectral properties. However, the observed fluxes and colours of galaxies are observed to depend on inclination, especially for spiral galaxies (e.g., Maller et al. 2009). SDSS galaxies have been morphologically classified using the concentration index C, defined as the ratio of the radii enclosing 90 per cent and 50 per cent of the r-band luminosity (e.g. Shimasaku et al. 2001; Strateva et al. 2001). We find that 64 per cent of the galaxies in our sample have concentration indices typical of late-type galaxies (i.e., $C < 2.6$). Thus, we must check that inclination effects do not introduce any strong bias in the results of Section 4.

We use the ratio b/a of minor to major axes of the SDSS r-band isophote at 25 mag arcsec^{-2} as a proxy for disc inclination. This is justified by the way in which galaxy ultraviolet and optical colours correlate with b/a. For example, we find that colours such as $g-r$ and $NUV-r$ correlate significantly with b/a, with the smaller b/a (presumably tracing higher disc inclinations) corresponding to the redder ultraviolet/optical colours. In Fig. 9, we plot several properties of the galaxies in the high-S/N subsample (Section 4) against the axis ratio b/a: apparent r-band magnitude, r; stellar mass, M_*; star formation rate averaged over the last 10^8 yr, ψ; total infrared luminosity[8], $L_{\rm d}^{\rm tot}$; dust mass, $M_{\rm d}$; and fraction of $L_{\rm d}^{\rm tot}$ contributed by dust in the diffuse ISM, f_μ.

We first highlight a selection effect: at low b/a (i.e. high inclination), the sample includes almost no galaxy fainter than $r \sim 16$ mag (Fig. 9a). This is because of the combined requirements of infrared detection by *IRAS* and ultraviolet detection by *GALEX*: edge-on galaxies in our sample must be optically bright

[8] We note that the values of $L_{\rm d}^{\rm tot}$ derived from our multi-wavelength analysis are typically 0.2 dex larger than those computed using the simple empirical approximation of eqs. (1)–(2).

enough that the limited relative dust content required for some ultraviolet photons to escape in the plane of the disc be also sufficient to warrant detection in the infrared. It is important to note that our restriction to the high-S/N subsample in Fig. 9a explains the lack of galaxies at the faintest magnitudes near the $r = 17.77$ selection cut-off even at low inclinations.

Fig. 9b shows that the median-likelihood estimates of stellar mass do not vary significantly with axis ratio, implying that inclination has a negligible influence on M_* constraints. This is not surprising, since constraints on M_* are dominated by the near-infrared emission, which is little sensitive to dust attenuation. Estimates of the star formation rate exhibit a stronger dependence on inclination (Fig. 9c): the typical ψ of face-on galaxies ($b/a \approx 1$) is a factor of about 3 larger than that of edge-on galaxies. This difference is significant when compared to the median confidence interval in ψ estimates (indicated on the figure). It is consistent with the selection bias identified in Fig. 9a against very dusty edge-on galaxies. This effect is also responsible for the lower dust masses and dust luminosities derived for edge-on compared to face-one galaxies in Figs. 9d and 9e. Finally, Fig. 9f shows the contribution f_μ to the total infrared luminosity by dust in the diffuse ISM is systematically higher in edge-on galaxies than in face-on ones. This is likely to result from the lower typical specific star formation rate of edge-on galaxies (Figs. 9b and 9c; see the correlation between f_μ and $\psi_{\rm S}$ in the right-most panels of Fig. 6).

We emphasise that the effects identified above are weak compared to the typical dispersion in the estimated parameters. Thus, inclination effects can account only for a minor fraction of the intrinsic scatter in the relations studies in Section 4.

5.3 Contamination by AGN hosts

In Section 3, we have interpreted the spectral energy distributions of galaxies in the matched *GALEX*-SDSS-2MASS-*IRAS* sample using the model of da Cunha et al. (2008). An important limitation of this model is that it does not include the potential contribution by an AGN to the infrared emission of a galaxy (e.g. de Grijp et al. 1985). For this reason, in Section 2, we have excluded from our sample all potential AGN hosts on the basis of their optical-line emission. However, optically-thick AGNs would not be eliminated using this method. This question is a fair concern, as the fraction of AGN hosts is known to increase with the total infrared luminosity (Veilleux et al. 1995; Cao et al. 2006). In addition, evidence for dust-enshrouded AGN activity has been found in some ULIRGs and LIRGs of the *IRAS* catalogue (Dudley & Wynn-Williams 1997; Imanishi & Dudley 2000). In an infrared-selected sample of high-redshift ($z \sim 0.8$) galaxies with infrared luminosities similar to those of the galaxies in our sample, Elbaz et al. (2002) find 12 ± 5 per cent (5/41) of AGN hosts based on available observations with *Chandra X-ray Observatory* (Brandt et al. 2001; Hornschemeier et al. 2001). It is conceivable, therefore, that a similar fraction of galaxies in our sample host an obscured AGN.

Hot dust in the torus surrounding an obscured AGN is expected to radiate mostly in the mid-infrared. This should have only a minor influence on our analysis, since most galaxies in our sample are not detected in the *IRAS* 12- and 25-μm bands (Fig. 6). However, some studies suggest that AGNs may be also contribute significantly to the far-infrared emission from galaxies. For example, in the analysis of a matched sample of SDSS-DR2 and *IRAS* galaxies, Pasquali et al. (2005) find that known AGN hosts exhibit a significant excess of 60- and 100-μm emission, amounting to a typical excess infrared luminosity of 0.18 dex. Yet, it remains unclear whether this excess emission arises from (cold) dust heated by the AGN or by a population of young stars not detected in the optical SDSS spectra. In another recent study, Salim et al. (2009) analyse the 24 μm emission of a sample of optically-selected galaxies observed with the *Spitzer Space Telescope* (Werner et al. 2004) out to redshift $z = 1.4$. They conclude that AGNs identified in the X-rays and the optical do not contribute significantly to the 24 μm emission in their sample. Moreover, optically selected AGNs do not present any evidence for an excess infrared luminosity, while obscured AGNs detected in the X-rays can contribute only up to 50 per cent of the total infrared luminosity.

We have checked that the possible excess infrared luminosity arising from an obscured AGN in these previous studies is within the typical confidence range of $L_{\rm d}^{\rm tot}$ estimates for the galaxies in our sample. We conclude that the potential contamination of the 60- and 100-μm *IRAS* flux densities by obscured AGNs would not alter significantly our conclusions.

5.4 Comparison with models of chemical and dust evolution

In this section, we compare the physical properties derived in Section 4 for the galaxies in the matched *GALEX*-SDSS-2MASS-*IRAS* sample with the predictions of chemical evolution models including the formation and destruction of dust grains in the ISM. We focus on the recent models of the chemical and dust evolution of galaxies in a wide range of star formation histories by Calura et al. (2008). These models, which are based on the formalism developed by Dwek (1998), include the production of dust in the cold envelopes of low- and intermediate-mass stars during the AGB phase and in the expanding ejecta of type-II and type-Ia supernovae. Dust grains are destroyed mainly by shock waves caused by supernovae explosions. The Calura et al. (2008) models allow one to compute the evolution of the stellar and dust masses of galaxies as a function of the star formation history.

We are particularly interested here in the Calura et al. (2008) models for the solar neighbourhood and for a dwarf-irregular galaxy with continuous star formation. The solar-neighbourhood model aims at reproducing the properties of the Galactic-disc component in a 2 kpc-wide ring located at 8 kpc from the Galactic centre. In this model, which assumes gas infall but no outflow, the Galactic disc is formed in two main episodes. The exact expression of the star formation history, taken from Chiappini et al. (1997), is essentially a function of the gas surface mass density with a critical threshold for star formation. In the model of dwarf-irregular galaxy, the star formation rate is expressed as a Schmidt-Kennicutt law and increases continuously with time. This model assumes gas infall and galactic winds. We refer the reader to the original paper of Calura et al. (2008) for more detail on these models.

In Fig. 10, we compare the median-likelihood estimates of $M_{\rm d}/M_*$ and $M_{\rm d}/\psi$ as a function of $\psi_{\rm S}$ for the galaxies in the high-S/N subsample of Section 4 with the predictions of the solar-neighbourhood model (red filled squares) and the dwarf-irregular galaxy model (blue filled circles) of Calura et al. (2008), at ages between 1 and 12 Gyr. At late ages, both models coincide remarkably well with the range of derived physical parameters of the *GALEX*-SDSS-2MASS-*IRAS* galaxies. The solar-neighbourhood model of Calura et al. (2008) does not include any bulge component. To locate the Milky Way in Fig. 10, we add to this model a bulge stellar mass of $1/3$ that of the disc. We assume that this bulge component has negligible contributions to $M_{\rm d}$ and $\psi_{\rm S}$ (consistent with the chemical evolution model of a 12-Gyr old spheroidal galaxy by Pipino et al. 2005). The resulting Milky-Way model has a total stel-

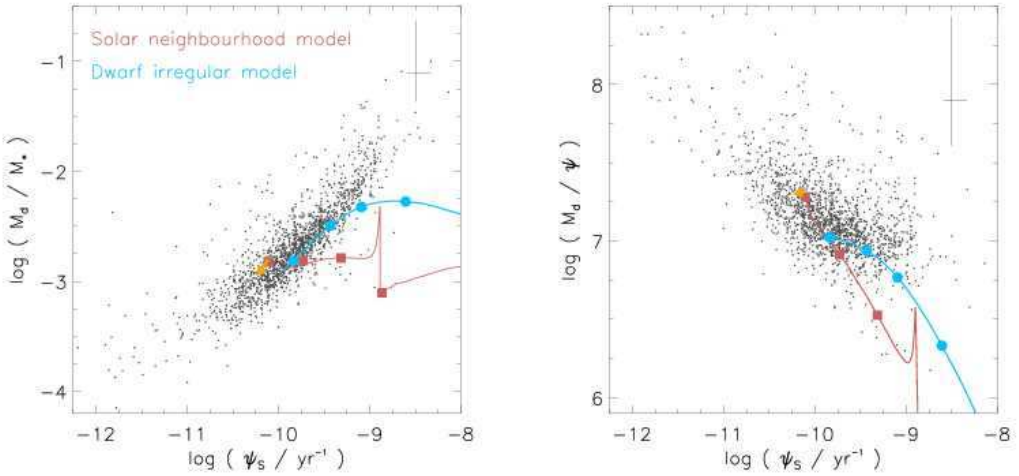

Figure 10. Comparison of the physical properties derived in Section 4 for the high-S/N galaxies in the matched *GALEX*-SDSS-2MASS-*IRAS* sample described in Section 2 (grey points) with the theoretical predictions of the Calura et al. (2008) models of chemical and dust evolution. *Left*: dust-to-stellar mass ratio $M_{\rm d}/M_*$ as a function of specific star formation rate $\psi_{\rm S}$. *Right*: ratio of dust mass to star formation rate $M_{\rm d}/\psi$ as a function of $\psi_{\rm S}$. The evolution of the solar-neighbourhood model of Calura et al. (2008) is shown in red, and that of the dwarf-irregular galaxy model in blue. Symbols indicate the locations of these models at ages 1, 3, 6 and 12 Gyr. The orange arrow shows the effect of adding a bulge component to the 12-Gyr old solar-neighbourhood model to mimic the Milky-Way properties (see text for detail).

lar mass $M_* = 4 \times 10^{10}\ M_\odot$, a star formation rate $\psi = 2.3\ M_\odot$ yr^{-1} and a dust mass $M_{\rm d} = 4.5 \times 10^7\ M_\odot$ (head of the orange arrow in Fig. 10). These parameters are typical of moderately star-forming and moderately dusty galaxies in our sample.

A valuable feature of the models shown in Fig. 10 is that they provide a framework to interpret the time evolution of the ISM properties of galaxies. Both the solar-neighbourhood and the dwarf-irregular galaxy models predict that, overall, $M_{\rm d}/M_*$ should drop and $M_{\rm d}/\psi$ should rise as the specific star formation rate $\psi_{\rm S}$ declines. These trends, and the good general agreement of the models with the derived physical properties of the galaxies in our sample in Fig. 10, suggest that the relations identified between $M_{\rm d}/M_*$, $M_{\rm d}/\psi$, f_μ and $\psi_{\rm S}$ in Section 4 (Fig. 6) may be the result, at least in part, of an evolutionary sequence. In detail, the interpretation of this sequence depends on several key assumptions of the chemical evolution models, such as the star formation history, the influence of gas infall and outflow, and the dust production and destruction rates. In the Calura et al. (2008) models of Fig. 10 (which both include gas infall, the dwarf irregular model also including gas outflow), a young galaxy has an ISM characterized by large amounts of dust-poor gas and forms stars at a very high rate. As the galaxy continues to consume gas into star formation, the stellar mass rises and the star formation rate declines, causing $\psi_{\rm S}$ to drop. The dust mass increases steeply during the first billion years of evolution, when the star formation rate is highest and large amounts of dust are produced in supernova ejecta and in the envelopes of AGB stars. As star formation drops, the dust mass $M_{\rm d}$ also drops, because the production of new dust grains cannot balance any more their destruction in the ISM. This general picture, which is consistent with our results, is also in broad agreement with the predictions of simple closed-box chemical evolution models (e.g., Dwek et al. 2000; Edmunds 2001).

6 SUMMARY AND CONCLUSION

In this paper, we have assembled a sample of 3258 local galaxies with photometric observations from at ultraviolet, optical and infrared wavelengths. These galaxies were primarily selected from the SDSS DR6 spectroscopic sample cross-correlated with *IRAS* all-sky catalogues (which are flux-limited at 60 μm). The optical and infrared observations were supplemented with matched ultraviolet and near-infrared data from *GALEX* and 2MASS, respectively. The size of this sample represents a significant improvement over previous multi-wavelength studies of galaxies. We have used the model of da Cunha et al. (2008) to interpret the observed spectral energy distributions of the galaxies in this sample in terms of statistical constraints on the star formation rate, stellar mass, dust attenuation, dust luminosity, fraction of dust luminosity contributed by the diffuse ISM, and dust mass.

We have focused on a subsample of 1658 galaxies with highest-S/N photometry to investigate several significant correlations between various derived physical properties of galaxies. In particular, we find that the star formation rate averaged over the last 10^8 yr, ψ, correlates remarkably well with galaxy dust mass $M_{\rm d}$ over 4 orders of magnitude in both quantities. The simple empirical recipe $M_{\rm d} = (1.28 \pm 0.02) \times 10^7\ (\psi/M_\odot\ {\rm yr}^{-1})^{1.11 \pm 0.01}\ M_\odot$ may be used to roughly estimate the total dust mass of a galaxy as a function of the star formation rate. We also find that the dust-to-stellar mass ratio $M_{\rm d}/M_*$, the ratio of dust mass to star formation rate $M_{\rm d}/\psi$ and the fraction f_μ of dust luminosity $L_{\rm d}^{\rm tot}$ contributed by the diffuse ISM correlate strongly with the specific star formation rate $\psi_{\rm S}$ for the galaxies in the high-S/N subsample. Some of these trends had already been anticipated in the analysis of a much smaller sample of 66 SINGS galaxies by da Cunha et al. (2008).

To investigate the origin of these correlations between various physical properties of galaxies, we have compared our results with the predictions of recent models of chemical and dust evolution of galaxies with different star formation histories by Calura et al. (2008). We conclude from this comparison that the relations

between $M_{\rm d}/M_*$, $M_{\rm d}/\psi$, f_μ and $\psi_{\rm S}$ could arise, at least in part, from an evolutionary sequence. As galaxies form stars, their ISM becomes enriched in dust, while the drop in gas supply makes the specific star formation rate decrease. Interestingly, as a result, a young, actively star-forming galaxy with low dust-to-gas ratio may still be highly dusty (in the sense of a high $M_{\rm d}/M_*$) because it contains large amounts of interstellar gas (Fig. 6). This may be important for the interpretation of the infrared emission from young, gas-rich star-forming galaxies at high redshift.

The results presented in this paper should be especially useful to improve the treatment of the ISM properties of galaxies in semi-analytic models of galaxy formation. More specifically, the results of Section 4 provide interesting constraints on the relation between star formation activity and dust content in such models. For example, the derived relation between $M_{\rm d}$ and ψ (Fig. 5) can be used in combination of the Schmidt-Kennicutt law (Schmidt 1959; Kennicutt 1998a) to describe the evolution of the dust content of galaxies together with that of the stars and gas. Also, the correlation between $\psi_{\rm S}$ and f_μ (Fig. 6) provides valuable clues on the way in which to implement the modelling of the different phases of the ISM in simulated galaxies.

Our study provides a local reference for comparison with the properties of galaxies at high redshifts. Observations with the *Spitzer* satellite have shown that infrared galaxies dominate the star formation activity of the universe at redshift $z \sim 1$ (Le Floc'h et al. 2005). Moreover, dust emission has been detected at submillimetre wavelengths out to $z \sim 6$, implying large dust masses and star formation rates of the order of several $\times 10^3\,M_\odot\,{\rm yr}^{-1}$ in (at least some) young galaxies (e.g., Chini & Kruegel 1994; Isaak et al. 2002; Blain et al. 2002; Bertoldi et al. 2003; Walter 2009). The production of such large amounts of dust on short timescales might require both efficient star formation and efficient grain condensation in supernova remnants (e.g., Dunne et al. 2003; Morgan & Edmunds 2003; Maiolino et al. 2004). This could affect the relation between star formation rate and dust mass. Forthcoming observations with the *Herschel Space Telescope* and the *James Webb Space Telescope* will enable the extension to high redshift of the type of analysis achieved in this paper. This can only lead to an improved understanding of the cosmic evolution of the dust content of galaxies.

ACKNOWLEDGEMENTS

We thank the referee, Charlie Conroy, for comments and suggestions which helped improve the quality of this paper. We are deeply grateful to David Schiminovich for matching the SDSS-*IRAS* sample with the latest *GALEX* data release and for kindly providing us with these data. We thank Jarle Brinchmann for useful discussions and for providing us with the corrections to account for emission-line contamination in the optical SDSS bands. We also thank Loretta Dunne, David Elbaz, Vivienne Wild, Jakob Walcher and Brent Groves for useful discussions. We thank Francesco Calura and Antonio Pipino for providing us with the electronic data of their chemical evolution models. EdC was financed by the EU Marie Curie Research Training Network MAGPOP and by the EU Marie Curie ToK Grant MTKD-CT-2006-039965. CE was supported by the Marie Curie EARA-EST host fellowship while this work was carried out and acknowledges the IAP for hospitality. CE is partly supported by the Swiss Sunburst Fund.

Funding for the SDSS has been provided by the Alfred P. Sloan Foundation, the Participating Institutions, the National Science Foundation, the US Department of Energy, the National Aeronautics and Space Administration, the Japanese Monbukagakusho, the Max Planck Society, and the Higher Education Funding Council for England. The SDSS Web site is http://www.sdss.org. The SDSS is managed by the Astrophysical Research Consortium for the Participating Institutions. The Participating Institutions are the American Museum of Natural History, the Astrophysical Institute Potsdam, the University of Basel, Cambridge University, Case Western Reserve University, the University of Chicago, Drexel University, Fermilab, the Institute for Advanced Study, the Japan Participation Group, Johns Hopkins University, the Joint Institute for Nuclear Astrophysics, the Kavli Institute for Particle Astrophysics and Cosmology, the Korean Scientist Group, the Chinese Academy of Sciences, Los Alamos National Laboratory, the Max Planck Institute for Astronomy, the Max Planck Institute for Astrophysics, New Mexico State University, Ohio State University, the University of Pittsburgh, the University of Portsmouth, Princeton University, the US Naval Observatory, and the University of Washington.

REFERENCES

Adelman-McCarthy et al. 2008, ApJS, 175, 297
Armus et al. 2007, ApJ, 656, 148
Baldwin J. A., Phillips M. M., Terlevich R., 1981, PASP, 93, 5
Beichman C. A., Neugebauer G., Habing H. J., Clegg P. E., Chester T. J., eds, 1988, Infrared astronomical satellite (IRAS) catalogs and atlases. Volume 1: Explanatory supplement Vol. 1
Bertoldi F., Carilli C. L., Cox P., Fan X., Strauss M. A., Beelen A., Omont A., Zylka R., 2003, A&A, 406, L55
Blain A. W., Smail I., Ivison R. J., Kneib J.-P., Frayer D. T., 2002, Physics Reports, 369, 111
Blanton et al. 2003, AJ, 125, 2348
Brandt W. N., Hornschemeier A. E., Alexander D. M., Garmire G. P., Schneider D. P., Broos P. S., Townsley L. K., Bautz M. W., Feigelson E. D., Griffiths R. E., 2001, AJ, 122, 1
Brinchmann J., Charlot S., White S. D. M., Tremonti C., Kauffmann G., Heckman T., Brinkmann J., 2004, MNRAS, 351, 1151
Bruzual G., 2007, (astro-ph/0703052)
Bruzual G., Charlot S., 2003, MNRAS, 344, 1000
Calura F., Pipino A., Matteucci F., 2008, A&A, 479, 669
Cao C., Wu H., Wang J.-L., Hao C.-N., Deng Z.-G., Xia X.-Y., Zou Z.-L., 2006, Chinese Journal of Astronomy and Astrophysics, 6, 197
Chabrier G., 2003, PASP, 115, 763
Charlot S., Fall S. M., 2000, ApJ, 539, 718
Chiappini C., Matteucci F., Gratton R., 1997, ApJ, 477, 765
Chini R., Kruegel E., 1994, A&A, 288, L33
Conroy C., White M., Gunn J. E., 2009, ArXiv e-prints
da Cunha E., Charlot S., Elbaz D., 2008, MNRAS, 388, 1595
de Grijp M. H. K., Miley G. K., Lub J., de Jong T., 1985, Nature, 314, 240
Dopita M. A., Groves B. A., Fischera J., Sutherland R. S., Tuffs R. J., Popescu C. C., Kewley L. J., Reuland M., Leitherer C., 2005, ApJ, 619, 755
Draine B. T., Dale D. A., Bendo G., et al. 2007, ApJ, 663, 866
Dudley C. C., Wynn-Williams C. G., 1997, ApJ, 488, 720
Dunne L., Eales S., Edmunds M., Ivison R., Alexander P., Clements D. L., 2000, MNRAS, 315, 115
Dunne L., Eales S., Ivison R., Morgan H., Edmunds M., 2003, Nature, 424, 285

Dwek E., 1998, ApJ, 501, 643
Dwek E., Fioc M., Varosi F., 2000, in D. Lemke, M. Stickel, & K. Wilke ed., ISO Survey of a Dusty Universe Vol. 548 of Lecture Notes in Physics, Berlin Springer Verlag, The Effect of Dust Evolution on the Spectral Energy Distribution of Galaxies. pp 157–+
Edmunds M. G., 2001, MNRAS, 328, 223
Elbaz D., Cesarsky C. J., Chanial P., Aussel H., Franceschini A., Fadda D., Chary R. R., 2002, A&A, 384, 848
Helou G., Khan I. R., Malek L., Boehmer L., 1988, ApJS, 68, 151
Hildebrand R. H., 1983, QJRAS, 24, 267
Hopkins A. M., Connolly A. J., Haarsma D. B., Cram L. E., 2001, AJ, 122, 288
Hornschemeier A. E., Brandt W. N., Garmire G. P., Schneider D. P., Barger A. J., Broos P. S., Cowie L. L., Townsley L. K., Bautz M. W., Burrows D. N., Chartas G., Feigelson E. D., Griffiths R. E., Lumb D., Nousek J. A., Ramsey L. W., Sargent W. L. W., 2001, ApJ, 554, 742
Imanishi M., Dudley C. C., 2000, ApJ, 545, 701
Isaak K. G., Priddey R. S., McMahon R. G., Omont A., Peroux C., Sharp R. G., Withington S., 2002, MNRAS, 329, 149
Isobe T., Feigelson E. D., Akritas M. G., Babu G. J., 1990, ApJ, 364, 104
Issa M. R., MacLaren I., Wolfendale A. W., 1990, A&A, 236, 237
Kauffmann et al. 2003a, MNRAS, 341, 33
Kauffmann et al. 2003b, MNRAS, 341, 54
Kennicutt Jr. R. C., 1998a, ARA&A, 36, 189
Kennicutt Jr. R. C., 1998b, ApJ, 498, 541
Kennicutt Jr. R. C., Armus L., Bendo G., Calzetti D., Dale D. A., Draine B. T., Engelbracht C. W., Gordon K. D., et al. 2003, PASP, 115, 928
Kewley L. J., Jansen R. A., Geller M. J., 2005, PASP, 117, 227
Kong X., Charlot S., Brinchmann J., Fall S. M., 2004, MNRAS, 349, 769
Le Floc'h E., Papovich C., Dole H., et al. 2005, ApJ, 632, 169
Lisenfeld U., Ferrara A., 1998, ApJ, 496, 145
Maiolino R., Schneider R., Oliva E., Bianchi S., Ferrara A., Mannucci F., Pedani M., Roca Sogorb M., 2004, Nature, 431, 533
Maller A. H., Berlind A. A., Blanton M. R., Hogg D. W., 2009, ApJ, 691, 394
Marigo P., Girardi L., 2007, A&A, 469, 239
Martin et al. 2005, ApJ, 619, L1
Morgan H. L., Edmunds M. G., 2003, MNRAS, 343, 427
Morrissey et al. 2005, ApJ, 619, L7
Moshir M., 1989, IRAS Faint Source Survey, Explanatory supplement version 1 and tape. Pasadena: Infrared Processing and Analysis Center, California Institute of Technology, 1989, edited by Moshir, M.
Obrić M., Ivezić Ž., Best P. N., Lupton R. H., Tremonti C., Brinchmann J., Agüeros M. A., et al. 2006, MNRAS, 370, 1677
Pasquali A., Kauffmann G., Heckman T. M., 2005, MNRAS, 361, 1121
Pipino A., Kawata D., Gibson B. K., Matteucci F., 2005, A&A, 434, 553
Rigopoulou et al. 1999, in Cox P., Kessler M., eds, The Universe as Seen by ISO Vol. 427 of ESA Special Publication, Ultraluminous IRAS galaxies as seen with ISO. pp 833–+
Salim S., Dickinson M., Rich R. M., Charlot S., Lee J. C., Schiminovich D., Perez-Gonzalez P. G., Ashby M. L. N., Papovich C., Faber S. M., Ivison R. J., Frayer D. T., Walton J. M., Weiner B. J., Chary R.-R., Bundy K., Noeske K., Koekemoer A. M., 2009, ArXiv e-prints
Salpeter E. E., 1955, ApJ, 121, 161
Saunders et al. 2000, MNRAS, 317, 55
Schlegel D. J., Finkbeiner D. P., Davis M., 1998, ApJ, 500, 525
Schmidt K.-H., Boller T., 1993, Astronomische Nachrichten, 314, 361
Schmidt M., 1959, ApJ, 129, 243
Seibert et al. 2005, ApJ, 619, L55
Shimasaku K., Fukugita M., Doi M., Hamabe M., Ichikawa T., Okamura S., Sekiguchi M., Yasuda N., Brinkmann J., Csabai I., Ichikawa S., Ivezić Z., Kunszt P. Z., Schneider D. P., Szokoly G. P., Watanabe M., York D. G., 2001, AJ, 122, 1238
Silva L., Granato G. L., Bressan A., Danese L., 1998, ApJ, 509, 103
Skrutskie et al. 2006, AJ, 131, 1163
Soifer B. T., Sanders D. B., Madore B. F., Neugebauer G., Danielson G. E., Elias J. H., Lonsdale C. J., Rice W. L., 1987, ApJ, 320, 238
Strateva et al. 2001, AJ, 122, 1861
Sullivan M., Mobasher B., Chan B., Cram L., Ellis R., Treyer M., Hopkins A., 2001, ApJ, 558, 72
Tremonti et al. 2004, ApJ, 613, 898
Veilleux S., Kim D.-C., Sanders D. B., 1999, ApJ, 522, 113
Veilleux S., Kim D.-C., Sanders D. B., Mazzarella J. M., Soifer B. T., 1995, ApJS, 98, 171
Walter F., 2009, ArXiv e-prints
Wang B., Heckman T. M., 1996, ApJ, 457, 645
Werner M. W., Roellig T. L., Low F. J., Rieke G. H., Rieke M., Hoffmann W. F., Young E., Houck J. R., 2004, ApJS, 154, 1